XCHEM Approach to the Ionization of Pyrazine

Pedro Fernández Milán

Máster en Química Teórica
y Modelización Computacional

MÁSTERES
DE LA UAM
2017 - 2018

Facultad de Ciencias

UAM Universidad Autónoma de Madrid

Master in

Theoretical Chemistry and Computational Modelling

XCHEM Approach to the Ionization of Pyrazine

Pedro Fernández Milán

Master Thesis. Course 2017-2018

Director: Fernando Martín García
Codirector: Jesús González Vázquez
Place where the project was carried out: Departamento de Química

Universidad Autónoma de Madrid

UNIVERSIDAD AUTÓNOMA DE MADRID

Abstract

Facultad de Ciencias
Departamento de Química

Master Thesis

XCHEM Approach to the Ionization of Pyrazine

by Pedro Fernández Milán

In this contribution we have studied the photoionization of pyrazine using the XCHEM method and compare it with a well-establish DFT approach. In this case, single channel single reference calculations were performed for several angular momenta of the ejected electron with both techniques. Finally, multichannel scattering cross sections were calculated with single reference and multireference methods. These simulations, which describe the effect of the electron correlation in the configurational interaction picture, were used to understand the photoionization cross sections of pyrazine. With the results of single reference and multireference calculations, we can estimate the importance of electron correlation in the description of the bound states and when single channel calculation and multichannel calculations are compared, we can observe the effect of coupling several electronic continua.

Acknowledgements

I would like to express my gratitude to the people that has made this possible

- My supervisors, Fernando and Jesús.
- Markus.
- IFIMAC.
- TCCM Programme.
- My family.

Contents

Chapter 1

Introduction

Since the discovery of electrons in the beginning of the 20th century humanity has undergone an unprecedented scientific and technological progress. Among all the achievements stand out the development of Quantum Theory that has allowed us to better understand the structure of matter and the transistor, considered by many the greatest invention of the 20th century and the foundation of modern electronics. Therefore, it is normally stated that the 20th century was the electron age. However, there is a strong believe that photons will hold a higher importance than electrons in the years to come. Still, as it is stated in [1], electron dynamics is responsible of many important processes, not just in physics; but also in chemistry and biology: light emission, charge transfer... Thus, controlling electron dynamics would bestow us a subtle control over such processes. Nevertheless, control at the atomic scale is still in early stages, so there is still much to do. This Master thesis is about uncovering the mysteries of electron dynamics in photoionization processes through the recent advances in laser technology.

In order to control electron motion, first we need to know the timescale at which they move, i.e., the time interval between electron snapshots that would allow to obtain a movie of the motion of an electron without losing information. Taking the Bohr model as a simple example, we could determine that the period of the first orbit is about 152 as ($10^{-18}s$). This is the timescale that would be necessary to reach in order to study electron dynamics.

The timescale at which a given system moves can be understood by considering a simple two-level system [1]. The larger the difference between energy levels the lesser the oscillating period. This is the reason why nuclei and electrons are in different timescales. In the case of nuclei, they move due to vibrations, and the vibrational levels of a molecule are quite close in energy comparing with electrons. Nuclei move in the femtosecond timescale (10^{-15} s) via vibrations, giving rise to chemical reactions. This is the area of study of femtochemistry, introduced by

Zewail [2, 3], who managed to study chemical reactions via pump-probe experiments with femtosecond lasers. With regard to imaging and controlling electron dynamics, it is required to break the barrier of the femtosecond. However, it was not until the appearance of attosecond lasers via High Harmonic Generation (HHG) [4] that this was made possible, giving rise to the promising attochemistry field [5].

The theoretical study of photoionization requires a good description of the electron continuum. However, quantum chemistry methods, that have nowadays become routine to describe bound electronic states with great accuracy, are not valid for the continuum. It is then necessary to provide similar tools to describe ionization processes so that increasingly sophisticated experiments can be explained. Several approaches have been developed along the years, from the single active electron approximation (SAE) to the static-exchange approximation (SEA) [6–8]. In the SEA approximation, the coupling between continuum states associated with different parent ions is neglected. This is usually the starting point of more sophisticated treatments based on the close-coupling (CC) approximation [9], where the coupling between different channels is included. The SEA is able to describe primary photoemission from valence shells or core orbitals in which the ejected photoelectron has energies bigger than 10 eV but having problems when more than one electron participates in the ionization, e.g. autoionization arising from multiply excited states.

To overcome the above limitations, our group has developed a different approach (XCHEM [10]) that matches the capability of state-of-the-art techniques for the calculation of correlated excited states, provided by widely available packages such as MOLCAS [11] and MOLPRO [12], with well-established techniques for the description of the electronic continuum. This is done by using a hybrid Gaussian-B-spline basis (GABS) [13].

There are other approaches based on a similar philosophy, in which a short-range part represented by GTOs is complemented with other functions more appropriate for the scattering description, such as finite-element (FE) representation of the radial coordinate [14, 15], discrete variable representation (DVR) [16] and plane waves [17]. Other efforts have been made within the framework of density functional theory (DFT), using for instance a multicenter expansion in B-splines [18]. Despite the existence of all these models, XCHEM has its own advantages. Increasing the number of electrons for a fixed number of scattering channels does not make the computational cost of the full dimensional problem significantly

higher. This means that the effort made to compute the helium atom would be similar to that needed to compute the water molecule for instance. Although this points to the fact that the computation of very small systems would not be very efficient, our real target, small and medium size molecules, would be easily achievable without serious penalties. Another benefit of this implementation is the capability to obtain from a multichannel scattering problem either time independent observables, e.g., resonance energies and widths, or time-dependent ones, expanding for the latter the wave function in the box of eigenstates, a very convenient way to carry out the time propagation and to extract observables from it. An additional advantage is that resonances, such as doubly excited states, arise naturally from the close-coupling expansion without the need of an ad hoc inclusion.

In this work we are focusing on the aromatic pyrazine molecule, the most complex system to which XCHEM methodology has been applied. We aim to obtain for the first time multichannel results for such system with a high level of accuracy of its electronic structure. We compare the results given by adapted single-channel XCHEM calculations with the ones obtained from the SEA based method [18, 19].

Chapter 2

Molecular Electronic Structure

2.1 The Schrödinger Equation

It has been long well known that Classical Physics does not describe correctly the behavior of atomic and molecular systems. Quantum Theory is necessary to tackle this issue, and of its most important results is the so-called Time Dependent Schrödinger Equation (TDSE) proposed by Erwin Schrödinger in the 20s. It is a partial diffusion-like linear and homogeneous differential equation. Being linear and homogeneous allow for the Superposition Principle, which states that if Ψ_1 and Ψ_2 are two solutions, then an arbitrary linear combination of both solutions is also a solution to the equation. It should also be highlighted the fact that it is first order with respect to time, meaning that one only has to specify the initial conditions of Ψ in order to know its evolution in time [20].

$$i\hbar\frac{\partial}{\partial t}\Psi(\vec{r},\vec{R},t) = \hat{H}(\vec{r},\vec{R},t)\Psi(\vec{r},\vec{R},t) \tag{2.1}$$

where Ψ is the wavefunction that holds all the information about the system and determines its dynamical state. $\hat{\mathrm{H}}$ is the Hamiltonian of the system under study, which consists of two parts: the kinetic energy of all the particles composing the system and the potential energy defining the system.

$$\hat{\mathcal{H}}(\vec{r},\vec{R},t) = \sum_{i}^{N} -\frac{\hbar^2}{2m_i}\nabla_i^2 + \mathcal{V}(\vec{r},t) \tag{2.2}$$

If one considers that $\mathcal{H}$ does not depend on time, one arrives at the Time Independent Schrödinger Equation (TISE), normally represented as follows

$$\hat{\mathcal{H}}\Psi_n = E_n\Psi_n \tag{2.3}$$

As it can be seen, this last equation consists of an eigenvalue problem, where E_n are the stationary energies of the system (eigenvalues) and Ψ_n the stationary wavefunctions (eigenvectors).

Quantum Chemistry is normally interested in molecules, which are composed of electrons and nuclei (we are not considering the internal structure of nuclei). We thus arrive at the Molecular Hamiltonian, in which one can distinguish the kinetic energy of electrons and nuclei and the different possible electrostatic interactions between them: electron-electron, electron-nuclei and nuclei-nuclei.

$$\hat{\mathcal{H}} = \mathcal{T}_e(\vec{r}) + \mathcal{T}_N(\vec{R}) + \mathcal{V}_{ee}(\vec{r}) + \mathcal{V}_{en}(\vec{r},\vec{R}) + \mathcal{V}_{nn}(\vec{R}) \tag{2.4}$$

$$\begin{aligned}\hat{\mathcal{H}} = & -\frac{1}{2}\sum_{i}^{N_e}\nabla_i^2 - \sum_{\alpha}^{N_n}\frac{1}{2M_\alpha}\nabla_\alpha^2 + \sum_{i=1}^{N_e}\sum_{j>i}^{N_e}\frac{1}{r_{ij}} \\ & + \sum_{i=1}^{N_e}\sum_{\alpha=1}^{N_n}\frac{Z_\alpha}{r_{i\alpha}} + \sum_{\alpha=1}^{N_n}\sum_{\beta>\alpha}^{N_n}\frac{Z_\alpha Z_\beta}{r_{\alpha\beta}}\end{aligned} \tag{2.5}$$

where 'n' and 'e' refer to nuclei and electron respectively. The number of degrees of freedom in this equation in which electrons and nuclei are coupled is astonishing. It is then impossible to solve exactly and one can obtain an approximate solution. The usual way of dealing with such equation is by assuming that nuclei remain fixed from the point of view of electrons, due to the former being much heavier. Thus, the nuclear kinetic energy can be neglected and the internuclear interaction energy becomes a constant since nuclei remain static. This is called the Born-Oppenheimer approximation (BOA), and allows to decouple electron and nuclear dynamics and reduce the dimensionality of the problem. Since we are considering the motion of electrons and nuclei to be independent, the total wavefunction of the system can be expressed as a direct product of an electronic and a nuclear part

$$\Psi = \psi(\vec{r};\vec{R})\varphi(\vec{R}) \tag{2.6}$$

Therefore, an electronic Hamiltonian $\mathcal{H}_e$ can be defined

$$\mathcal{H}_e = \mathcal{T}_e(\vec{r}) + \mathcal{V}_{ee}(\vec{r}) + \mathcal{V}_{ne}(\vec{r},\vec{R}) \tag{2.7}$$

The electronic wavefunction depends parametrically on the nuclear coordinates. This means that in order to fully solve the problem one has to obtain the electronic wavefunction for different nuclear configurations, obtaining what is referred to as a Potential Energy Surface (PES). In the case of diatomic molecules,

this PES is just a curve, since the only relevant nuclear coordinate is the nuclear distance.

In the sections that follow the most important methods for solving the Electronic Structure of molecules will be discussed.

2.2 Hartree-Fock Theory

It has already been stated that solving exactly the Molecular TISE is impossible. Therefore, approximations are needed in order to deal with such complexity. We have already introduced the BOA that allowed to work in a lower dimensionality. Nevertheless, even for a single nuclear configuration, the number of degrees of freedom continues being too large. That is why other approximations or models are needed to deal with the electronic TISE. Through the years, several methods have been developed in the computational chemistry community to obtain approximated electronic wavefunctions. The Hartree-Fock method is the father of other more accurate and sophisticated methods that will be reviewed later on and the outset of computational chemistry as a standalone discipline.

Hartree-Fock is a method for solving the electronic TISE within the BOA for a system of N_e electrons and N_n nuclei. Its core hypothesis consists on each electrons moving in the average potential created by the nuclei and the rest of N_e-1 electrons. As a result, it neglects what is termed correlation [21]. It is based on the variational method, meaning that it aims at minimizing the energy functional

$$E[\psi] = \frac{\langle \psi | \mathcal{H}_e | \psi \rangle}{\langle \psi | \psi \rangle} \tag{2.8}$$

thence we are looking for a many-electron wavefunction ψ such that the energy is minimum. This ensures that the calculated energy is always an upper bound to the exact ground state energy. Nonetheless, one cannot try all possible wavefunctions, but we must restrict ourselves to a subset of them.

$$|\psi\rangle = \frac{1}{\sqrt{N_e}} \begin{vmatrix} \chi_1(x_1) & \chi_2(x_1) & \cdots & \chi_{N_e}(x_1) \\ \chi_1(x_2) & \chi_2(x_2) & \cdots & \chi_{N_e}(x_2) \\ \vdots & \vdots & \ddots & \vdots \\ \chi_1(x_{N_e}) & \chi_2(N_e) & \cdots & \chi_{N_e}(x_{N_e}) \end{vmatrix} = |\chi_1 \chi_2 \cdots \chi_{N_e}\rangle \tag{2.9}$$

The trial functions we are considering as many-electron wavefunctions are single Slater determinants, since they ensure the antisymmetry of the wavefunction, i.e., the permutation of any two particles causes a change of sign in the wavefunction (Pauli principle). A Slater determinant, as seen in Equation 2.9, consists of an antisymmetrized product of N_e one-electron functions, or spin orbitals. The wavefunction depends, hence, on $4N_e$ variables; 3 spatial and 1 spin coordinate per spin orbital. Consequently, the energy E is a functional of the spin orbitals $\{\chi_i\}$ [22].

The derivation of the Hartree-Fock equations comes from applying the variational procedure to find the spin orbitals that minimize the ground state energy given by

$$E[\{\chi_i\}] = \langle\psi|\,\hat{\mathcal{H}}_e\,|\psi\rangle \tag{2.10}$$

$$= \langle\psi|\,-\frac{1}{2}\sum_{i}^{N_e}\nabla_i^2 - \sum_{i=1}^{N_e}\sum_{\alpha=1}^{N_n}\frac{Z_\alpha}{r_{i\alpha}} + \sum_{i=1}^{N_e}\sum_{j>i}^{N_e}\frac{1}{r_{ij}}\,|\psi\rangle \tag{2.11}$$

$$= \sum_{i=1}^{N_e}\langle\chi_1\cdots\chi_{N_e}|\,\hat{h}_i\,|\chi_1\cdots\chi_{N_e}\rangle + \sum_{i=1}^{N_e}\sum_{j>i}^{N_e}\langle\chi_1\cdots\chi_{N_e}|\,\frac{1}{r_{ij}}\,|\chi_1\cdots\chi_{N_e}\rangle \tag{2.12}$$

where we have defined the one-electron operator

$$\hat{h}_i = -\frac{1}{2}\nabla_i^2 - \sum_{\alpha}^{N_n}\frac{Z_\alpha}{r_{i\alpha}} \tag{2.13}$$

which represents the kinetic and potential energy of a single electron. The second term in Equation 2.12 contains, instead the two-electron operator $1/r_{ij}$. The total electronic hamiltonian is decomposed into a one- and two-electron contributions.

Considering that a determinant can be expressed as a sum of permutations over a product of spin orbitals [22]

$$|\chi_1\chi_2\cdots\chi_{N_e}\rangle = (N_e!)^{-1/2}\sum_{n=1}^{N_e!}(-1)^{p_n}\,\hat{\mathcal{P}}_n\{\chi_1\chi_2\cdots\chi_{N_e}\} \tag{2.14}$$

a set of rules for matrix elements of the form $\langle\psi|\,\hat{\mathcal{O}}\,|\psi'\rangle$; being ψ and ψ' two Slater determinants, not necessarily identical,can be derived [22]. The operator $\hat{\mathcal{O}}$ can be one- and two-electron, and is represented by $\hat{\mathcal{O}}_1$ and $\hat{\mathcal{O}}_2$ respectively. For a

one electron operator

$$\langle \Psi | \hat{\mathcal{O}}_1 | \Psi' \rangle = \begin{cases} \sum_{i=1}^{N_e} \langle \chi_i | \hat{\mathcal{O}}_1 | \chi_i \rangle & \text{if } \Psi = \Psi' \\ \langle \chi_n | \hat{\mathcal{O}}_1 | \chi'_n \rangle & \text{if } \Psi \text{ and } \Psi' \text{ differ in the n th orbital} \\ 0 & \text{if } \Psi \text{ and } \Psi' \text{ differ in more than one orbital} \end{cases} \tag{2.15}$$

In the case of the two-electron operator $\frac{1}{r_{12}}$ one obtains

$$\langle \psi | \hat{\mathcal{O}}_2 | \psi' \rangle = \begin{cases} \frac{1}{2} \sum_{i=1}^{N_e} \sum_{j=1}^{N_e} \langle \chi_i \chi_j | \frac{1}{r_{12}} | \chi_i \chi_j \rangle & \text{if } \Psi = \Psi' \\ \sum_{i=1}^{N_e} \langle \chi_n \chi_i | \frac{1}{r_{12}} | \chi'_n \chi_i \rangle & \text{if } \chi_n \neq \chi'_n \\ \langle \chi_n \chi_m | \frac{1}{r_{12}} | \chi'_n \chi'_m \rangle & \text{if } \chi_n \neq \chi'_n \text{ and } \chi_m \neq \chi'_m \\ 0 & \text{if } \Psi \text{ and } \Psi' \text{ differ in more than two orbitals} \end{cases} \tag{2.16}$$

In the case of HF, $\psi = \psi'$. The HF energy can then be written in terms one- and two-electron integrals involving the set of spin orbitals $\{\chi_i\}$. It can be seen as the sum of one-electron energies coming from electrons in spin orbital χ_i and interaction energies coming from electrons in spin orbitals χ_i and χ_j

$$E_{HF}[\{\chi_i\}] = \sum_{i=1}^{N_e} \langle \chi_i | \hat{h} | \chi_i \rangle + \frac{1}{2} \sum_{i}^{N_e} \sum_{j}^{N_e} \langle \chi_i \chi_j | \frac{1}{r_{12}} | \chi_i \chi_j \rangle \tag{2.17}$$

Finally, we want to minimize the energy from Equation 2.17 constraining the spin orbitals to be orthonormal, i.e.

$$\langle \chi_i | \chi_j \rangle = \delta_{ij} \tag{2.18}$$

$$\langle \chi_i | \chi_j \rangle - \delta_{ij} = 0 \tag{2.19}$$

In order to impose this constraint we make use of the Lagrange multipliers method, so that the functional to minimize is the following

$$\mathcal{L} = \sum_{i=1}^{N_e} \langle \chi_i | \hat{h} | \chi_i \rangle + \frac{1}{2} \sum_{i}^{N_e} \sum_{j}^{N_e} \langle \chi_i \chi_j | \frac{1}{r_{12}} | \chi_i \chi_j \rangle + \sum_{i}^{N_e} \sum_{j}^{N_e} \epsilon_{ij} (\langle \chi_i | \chi_j \rangle - \delta_{ij}) \tag{2.20}$$

where ϵ_{ij} are Lagrange multipliers, and represent the spin orbitals energy. By applying infinitesimal variations to spin orbitals so that

$$\chi_i \rightarrow \chi_i + \delta\chi_i \tag{2.21}$$

we obtain the first variation in $\mathcal{L}$

$$\begin{aligned}\delta\mathcal{L}[\{\delta\chi_i\}] =& \mathcal{L}[\chi_i + \delta\chi_i] - \mathcal{L}[\chi_i] \\ =& \sum_{i=1}^{N_e} \langle \delta\chi_i | \hat{h} | \chi_i \rangle + \sum_{i=1}^{N_e}\sum_{j=1}^{N_e} \langle \delta\chi_i\, \chi_j | \frac{1}{r_{12}} | \chi_i \chi_j \rangle \\ & - \sum_{i}^{N_e}\sum_{j}^{N_e} \epsilon_{ij}(\langle \delta\chi_i | \chi_j \rangle - \delta_{ij}) \\ & + \text{complex conjugate} = 0\end{aligned} \tag{2.22}$$

Given the fact that $\mathcal{L}$ is real, $\delta L = 0$ fulfills solely if

$$\left[\hat{h} + \sum_{j=1}^{N_e} \hat{\mathcal{J}}_j - \hat{\mathcal{K}}_j\right] \chi_i = \sum_{i=j}^{N} \epsilon_{ij}\chi_j \quad \text{for each i=1,2,...,}N_e \tag{2.23}$$

where $\hat{\mathcal{J}}$ and $\hat{\mathcal{K}}$ are one-electron operators. They are known as the coulomb and exchange operators respectively and are defined as

$$\hat{\mathcal{J}}_j(1)\chi_i(1) = \left\langle \chi_j \middle| \frac{1}{r_{12}} \middle| \chi_j \right\rangle_2 \chi_i(1) \tag{2.24}$$

$$\hat{\mathcal{K}}_j(1)\chi_i(1) = \left\langle \chi_j \middle| \frac{1}{r_{12}} \middle| \chi_i \right\rangle_2 \chi_j(1) \tag{2.25}$$

These operators are defined according to their action on a spin orbital χ_i.

The Hartree-Fock equations can be simplified if we define the square brackets in Equation 2.23 as Fock operator $\hat{f}$

$$\hat{f}\,|\chi_i\rangle = \sum_{j=1}^{N_e} \epsilon_{ij}\,|\chi_j\rangle \tag{2.26}$$

The Fock operator is a one-electron operator, meaning that it does not take into account electron correlation. The electronic interaction is accounted for only averagely. It can be demonstrated that the set of spin orbitals $\{\chi_i\}$ is not unique,

meaning that one can obtain a new set of spin orbitals by a unitary transformation. The new single determinant wavefunction is identical to the previous one except for a phase factor. In view of the fact that all observables depend on the square of the wavefunction, expectation values remain thus invariant.

Projecting the above Equation 2.23 onto spin orbital χ_k

$$\langle \chi_k | \hat{f} | \chi_i \rangle = \sum_{j}^{N_e} \epsilon_{ij} \langle \chi_k | \chi_i \rangle = \epsilon_{kj} \tag{2.27}$$

which means that the Lagrange multipliers ϵ are the matrix elements of the Fock operator. Taking into account what was stated about unitary transformations on spin orbitals, it is possible to find a suitable unitary transformation that makes the Fock operator diagonal; thence Equation 2.23 simplifies to

$$\hat{f} \, | \chi_i \rangle = \epsilon_i \, | \chi_i \rangle \tag{2.28}$$

The physical interpretation of the eigenvalues of the Fock operator ϵ_i was given by Koopmans, according to whom they could be seen as they necessary energy to remove an electron occupying spin orbital χ_i.

2.2.1 Roothan Equations. SCF procedure

The development of Hartree-Fock equations was an important leap, however, they are not solvable for systems of chemical interest, molecules, meaning that its applicability was reduced mainly to atoms [22]. This hurdle was overcome thanks to the work of Roothaan [23]. The forthcoming development of Roothaan's theory will be done under the restricted Hartree-Fock formalism, i.e. each spatial orbital is shared by two electron with opposite spins. Spin orbitals can then be factorized as follows

$$\chi_i = \Phi_i \alpha \tag{2.29}$$

$$\chi_i = \Phi_i \beta \tag{2.30}$$

In a closed shell system, there are the same number of α and β spins, meaning that the Slater determinant wavefunction depends only on spatial functions, and no longer on spin coordinates since they have been integrated out. The HF equation results to be

$$\hat{f}(r_1)\psi_i(r_1) = \epsilon_i \psi_i(r_1) \tag{2.31}$$

where r_1 are the spatial coordinates of one electron. The Fock operator is now expressed in terms of $N_e/2$, since for each spatial orbital Φ_i there are two electrons, with α and β spin

$$\hat{f} = \hat{h} + \sum_{i}^{N_e/2} 2\hat{\mathcal{J}}_i - \hat{\mathcal{K}}_i \tag{2.32}$$

The contribution of Roothaan was to employ a set of well known basis function in which to expand the spatial orbitals. This would allow to convert the integro-differential HF equations to a set of algebraic equations, much easily solvable by standard matrix techniques. Theoretically, the basis function should be able to expand the infinite $\mathcal{L}^2$ space, though in practice just a subset is enough for practical purposes. The unknown spatial orbitals, or molecular orbitals, are then expressed as a linear combination a N_b-dimensioned basis

$$\Phi_i = \sum_{\nu=1}^{N_b} c_{\nu i}\phi_\nu \tag{2.33}$$

We now introduce the molecular orbital expansion into Equation 2.31 to obtain

$$\hat{f}\sum_{\nu} c_{\nu i}\phi_\nu = \epsilon_i \sum_{\nu i} c_{\nu i}\phi_\nu \tag{2.34}$$

We project both sides of the previous equation onto $\langle\phi_\mu|$ to obtain

$$\sum_{\nu} c_{\nu i}\langle\phi_\mu|\hat{f}|\phi_\nu\rangle = \epsilon_i \sum_{\nu} c_{\nu i}\langle\phi_\mu|\phi_\nu\rangle \tag{2.35}$$

from where we can define:

- The overlap matrix **S** of dimension $N_b \times N_b$ and hermitian with elements

$$S_{\mu\nu} = \langle\phi_\mu|\phi_\nu\rangle = \int \mathrm{d}r_1\, \phi_\mu^*\phi_\nu \tag{2.36}$$

- The Fock matrix **F** also hermitian and with $N_b \times N_b$ dimension

$$F_{\mu\nu} = \langle\phi_\mu|\hat{f}|\phi_\nu\rangle = \int \mathrm{d}r_1\, \phi_\mu^*\hat{f}\phi_\nu \tag{2.37}$$

- The basis expansion coefficients matrix **C**, where column i contains the expansion coefficients for molecular orbital i, as seen in Equation 2.33

- The orbital energies matrix $\boldsymbol{\epsilon}$. It should be noted that it is a diagonal matrix of dimension $N_b \times N_b$, meaning that each element ϵ_{ii} corresponds to the energy of molecular orbital i.

The Roothaan equation can be written more elegantly in terms of these matrices as

$$\boldsymbol{FC} = \boldsymbol{SC\epsilon} \tag{2.38}$$

This equation can be transformed into the following eigenvalue problem, easier to solve computationally

$$\boldsymbol{F'C'} = \boldsymbol{C'\epsilon} \tag{2.39}$$

if we consider a transformation matrix that fulfills

$$\boldsymbol{X^\dagger SX} = \mathbf{1} \tag{2.40}$$

which means, that the **X** matrix orthonormalizes the overlap matrix. The new Fock and coefficients matrices are defined as

$$\boldsymbol{F'} = \boldsymbol{X^\dagger FX} \tag{2.41}$$

$$\boldsymbol{C'} = \boldsymbol{X^{-1}C} \tag{2.42}$$

We now define the density matrix **P** from the expression of the electron density for a single determinant wavefunction as follows

$$\rho(r) = 2\sum_{i}^{N_e/2} |\psi_i(r)|^2 \tag{2.43}$$

$$= 2\sum_{i}^{N_e/2}\sum_{\nu} c_{\nu i}^* \phi_\nu^* \sum_{\mu} c_{\mu i}\phi_\mu$$

$$= \sum_{\nu}\sum_{\mu} P_{\mu\nu}\phi_\nu^*\phi_\mu \tag{2.44}$$

where by inserting the molecular expansion 2.33 into Equation 2.43 and defining the matrix element

$$\mathbf{P}_{\mu\nu} = 2\sum_{i}^{N_e/2} c_{\mu i}c_{\nu i}^* \tag{2.45}$$

Equation 2.44 is obtained. The Fock matrix elements in terms of the density matrix have the following form

$$F_{\mu\nu} = h_{\mu\nu} + \sum_{\lambda\sigma} P_{\lambda\sigma}[\langle\mu\nu|\sigma\lambda\rangle - 1/2\,\langle\mu\lambda|\sigma\nu\rangle] \tag{2.46}$$

$$= h_{\mu\nu} + G_{\mu\nu} \tag{2.47}$$

where we distinguish a one electron part $h_{\mu\nu}$ and a two electron part $G_{\mu\nu}$. As one can notice, to solve the Roothaan equations means to obtain the energies and the coefficient matrix, or equivalently the density matrix. However, in order to do this one must first obtain the Fock matrix, which also depends on the density matrix. Consequently, Roothaan equations are nonlinear and must be solved by using the known as self consistent field (SCF). It consists of an iterative procedure that follows the next steps [22]:

1. Calculate one-electron integrals to build up **h** and **S** and two-electron integrals to build **G**. The one-electron matrices need only to be calculated once at the beginning of the procedure.
2. Diagonalize the **S** matrix and obtain the transformation matrix **X**
3. Guess an initial density matrix **P**.
4. Calculate **G** from two-electron integrals already computed at the beginning and the density matrix to obtain the Fock matrix **F**.
5. Compute the transformed Fock matrix $\mathbf{F}'$.
6. Diagonalize $\mathbf{F}'$ that results in $\boldsymbol{\epsilon}$ as eigenvalues and $\mathbf{C}'$ as eigenvectors, from which matrix **C** shall be computed.
7. With the new coefficients compute a new density matrix $\mathbf{P_{i+1}}$
8. If $|\mathbf{P}_{i+1} - \mathbf{P}_i| \geq \delta_{thr}$ recalculate the **G** matrix and follow the steps to obtain a new **P** matrix.

In summary, we have introduced a basis set of dimension N_b in which to expand the molecular orbitals Φ_i. This gives rise to an algebraic equation in terms of matrices of dimension $N_b \times N_b$, implying that one obtains as many molecular orbitals as basis functions used. Nevertheless, in the Slater determinant there are only $N_e/2$ molecular orbitals; therefore, the rest $N_b - N_e/2$ orbitals correspond to what is called virtual orbitals.

2.2.2 Basis sets

We have stated that Roothaan equations appear when one considers a basis set in which to expand the HF spatial orbitals. However, nothing has been said about the nature of this basis. A good basis set should follow these guidelines [24]:

- Allow for systematic extension to completeness. A complete description of the problem is only possible with an infinite basis that spans the whole $\mathcal{L}^2$.
- Rapid convergence, so that only a few terms are needed in the expansion to yield satisfactory results.
- Easy to manipulate analytical form for efficient evaluation of molecular integrals and if possible orthogonal.

In general, it is not possible to fulfill all the above requirements and one has to sacrifice some properties in exchange of others. It could be possible to have an orthonormal and analytic basis set, for example by using the eigenfunctions of the harmonic oscillator. However, this basis set would suffer from slow convergence.

Quantum chemistry normally uses an atomic centered non-orthonormal basis. There are various possible functional forms, but the most important ones are Slater type orbitals (STO), and especially Gaussian type orbitals (GTO). Slater type orbitals are obtained from the Hydrogen atom orbitals by truncating the Laguerre polynomial. In principle they are the most appropriate functions, due to their good convergence and ability to represent the nuclear cusp. However, STO hinder the calculation of molecular integrals, since they have to be computed numerically. On the other side, GTO provide analytical molecular integrals no matter the number of centers (atoms), since the product of two gaussian functions is always another gaussian function. For nothing is perfect, GTO suppose a worsening in convergence, meaning that more basis functions are needed to obtain reasonable results. Nonetheless, this has been partially solved by using gaussian contractions that mimic STOs.

2.3 Configuration Interaction

Although HF was a huge success, there were some problems inherent to the theory. Nevertheless, there has been much work over the last decades to improve

the HF wavefunction and overcome its shortcomings. Configuration interaction consists of an extension of HF theory that considers the following wavefunction

$$|\Psi_{CI}\rangle = c_0 |\Psi_0\rangle + C_S |S\rangle + C_D |D\rangle + C_T |T\rangle + C_Q |Q\rangle + \dots \tag{2.48}$$

where S,D,T... refer to all possible single, double, triple... excitations from the Hartree-Fock wavefunction, that is taken as the reference. This means we are supposing that the main contribution to Ψ_{CI} comes from the HF wavefunction Ψ_0 and the rest of Slater determinants behave as corrections. Excitation refers to the exchange of one or more occupied orbitals of the HF wavefunction for the same number of virtual orbitals.

The determination of the expansion coefficients is a linear variational problem, and as such, it is equivalent to diagonalizing the Hamiltonian in a basis of N-electron functions, i.e. excitations

$$\mathbf{HC} = E_{CI}\mathbf{C} \tag{2.49}$$

where **C** is the CI vector containing the coefficients of the expansion. The solution to the previous eigenvalue problem yields a set of eigenvectors and eigenvalues, being the lowest for the ground state and the rest for excited states. The Hamiltonian matrix to diagonalize has the next symmetric shape

$$\begin{pmatrix} \langle\Psi_0|\hat{\mathcal{H}}|\Psi_0\rangle & 0 & \langle\Psi_0|\hat{\mathcal{H}}|D\rangle & 0 & 0 & \cdots \\ & \langle S|\hat{\mathcal{H}}|S\rangle & \langle S|\hat{\mathcal{H}}|D\rangle & \langle S|\hat{\mathcal{H}}|T\rangle & 0 & \cdots \\ & & \langle D|\hat{\mathcal{H}}|D\rangle & \langle D|\hat{\mathcal{H}}|T\rangle & \langle D|\hat{\mathcal{H}}|Q\rangle & \cdots \\ & & & \langle T|\hat{\mathcal{H}}|T\rangle & \langle T|\hat{\mathcal{H}}|Q\rangle & \cdots \\ & & & & \langle Q|\hat{\mathcal{H}}|Q\rangle & \cdots \\ & & & & & \vdots \end{pmatrix} \tag{2.50}$$

The form of this matrix is consequence of the Brillouin theorem which states that single excitations and the reference ground state do not mix, giving $\langle\Psi_0|\hat{\mathcal{H}}|S\rangle = 0$. Regarding the remaining elements, it should be reminded that matrix elements between two different determinants that differ in more than two orbitals are zero. Considering a complete basis, one would obtain exact energies for the ground state and all excited states of the system.

This method provides lower energies than the HF method, meaning that we are able to recover correlation energy, defined as the difference between the exact

and HF energy

$$E_{corr} = E_{exact} - E_{HF} \tag{2.51}$$

The number of different Slater determinants that can be constructed given N_b one-electron basis functions and N_e electrons is

$$\binom{2N_b}{N_e} \tag{2.52}$$

making this scheme inapplicable to large systems, due to the huge configuration space that must be taken into account. The usual and most straightforward approach is to use a truncated CI wavefunction, instead of the full expansion, thus reducing the number of determinants that have to be considered. Truncation means that one only considers excitations up to certain order. We can distinguish then the CID, CISD... methods.

This approach allows for considering larger systems, but at the cost of losing size-consistency: the calculated energy does not follow a linear relationship with the number of particles. This has been solved by the development of Coupled Cluster Theory [25–27], which rather than a linear anstaz like CI uses an exponential anstz. However, this method is not variational.

2.4 Multiconfigurational Methods

Now we are going to consider methods that are not subject to the restriction of just one reference, as in the previous case where the orbitals used to generate the contribution came from a previous HF calculation. In the MCSCF technique the orbitals are optimized along with the CI vector. At the end of the calculation we obtain the best CI vector accompanied by the best orbitals that describe the system. This means that the set of orbitals affects the results, even if they are obtained just by rotations of the HF orbitals.

The MCSCF wavefunction is of CI type, and thus

$$|\psi\rangle = \sum_i c_i \left|{}^{2S+1}\Xi_i\right\rangle \tag{2.53}$$

where $\{{}^{2S+1}\Xi_i\}$ constitutes the space of Configuration State Functions (CSF). They

are spin-adapted functions with a defined multiplicity constructed from a suitable linear combination of Slater determinants

$$\left|{}^{2S+1}\Xi_i\right\rangle = \sum_n a_{ni} \left|D_n\right\rangle \tag{2.54}$$

There are several ways of constructing CSF, being the most widespread the Graphical Unitary Group Approach (GUGA) [28, 29]. Apart from well-defined spin, CSF give rise to smaller CI space since only spin-defined functions are used. On the contrary, the construction of operators requires to expand the CSF in the determinant space yielding

$$\left|\psi\right\rangle = \sum_i c_i \left|{}^{2S+1}\Xi_i\right\rangle \xrightarrow{GUGA} \sum_i c_i \sum_n a_{ni} \left|D_n\right\rangle = \sum_n d_n \left|D_n\right\rangle \tag{2.55}$$

where Slater-Condon rules from Equation 2.15 and Equation 2.16 can be applied.

We introduce the Hamiltonian in terms of annihilation and creator operators

$$\hat{\mathcal{H}} = \sum_{ij} \langle i|\hat{h}|j\rangle \, \hat{a_i}^\dagger \hat{a_j} + \frac{1}{2} \sum_{ijkl} \langle ij|kl\rangle \, \hat{a_i}^\dagger \hat{a_j}^\dagger \hat{a_k} \hat{a_l} \tag{2.56}$$

where i,j,k and l are molecular orbitals. The first term constitutes the one-electron integrals h_{ij}, while the second the two-electron integrals g_{ijkl}. The energy of the MCSCF wavefunction in the determinant basis is then

$$\begin{aligned} E &= \langle\psi|\hat{\mathcal{H}}|\psi\rangle && (2.57)\\ &= \sum_{ij} h_{ij} \sum_{nm} d_m^* d_n \, \langle D_m|\hat{a_i}^\dagger \hat{a_j}|D_n\rangle + \frac{1}{2} \sum_{ijkl} g_{ijkl} \sum_{mn} d_m^* d_n \, \langle D_m|\hat{a_i}^\dagger \hat{a_j}^\dagger \hat{a_k} \hat{a_l}|D_n\rangle && (2.58)\\ &= \sum_{ij} h_{ij} \sum_{mn} d_m^* d_n D_{ij}^{mn} + \sum_{ijkl} g_{ijkl} \sum_{mn} d_m^* d_n P_{ijkl}^{mn} && (2.59)\\ &= \sum_{ij} h_{ij} D_{ij} + \sum_{ijkl} g_{ijkl} P_{ijkl} && (2.60) \end{aligned}$$

with D_{ij} and P_{ijkl} the one and second order reduced density matrix elements respectively. The one and two electron integrals hold the information about the orbitals, while the reduced density matrices contain the CI coefficients.

It is not possible to consider the whole set of configurations, and one normally considers the subset of configurations that better describes the system. One of the most usual procedures to reduce the dimensionality of the configuration space is the so called complete active space (CAS) [30, 31], by which configurations are

selected by families. CAS divides the orbitals in three main groups: inactive, active and virtual. Excitations are only allowed in the active orbitals, resulting in a full CI in the active space. There are other possibilities for constructing the space of configurations. Special attention deserves RASSCF [32, 33], that grants more flexibility in selecting the relevant configurations. As well as distinguishing between inactive and virtual orbitals, it considers three spaces RAS1, RAS2 and RAS3. RAS2 is equivalent to the previously described CAS space. The flexibility is given by the RAS1 and RAS3 spaces. The former permits to excite a given number of electrons from orbitals that are not inactive enough to be considered as such while the latter is composed of a set of orbitals to which we allow a certain number of electrons to be excited to.

Obtaining several states for a given system could be as simple as making a calculation for each of the states we are looking for. However, this would result in a set of optimized states, each with its own CI vector, but also with a different set of orbitals. This can lead to what is called root-flipping. That is why, one normally computes a set of states under state-averaged formalism which aims at minimizing the average energy

$$E = \sum_I \omega_I \langle I|\mathrm{H}|I\rangle \tag{2.61}$$

over the pursued I states weighted by ω_I. The weights are normally chosen to be equal for all the states. This approach is termed as state-averaged CASSCF (SA-CASSCF) and is widely used in the XCHEM method.

CASSCF and RASSCF recover part of the correlation energy, so-called static correlation static correlation with a reasonable number of configurations. However, much more configurations are needed to describe the remaining correlation, known as dynamic. There are two ways of improving CASSCF and RASSCF on top of them. One possibility would be to consider all single and double excitations from all the determinants that take part in the MCSCF wavefunction. This approach is known as MRCI [34–36]. The other option is to make use of perturbation theory, for example the CASPT2 method [37].

2.5 Density Functional Theory

The appearance of Density Functional Theory (DFT) supposed a change of paradigm. Instead of concentrating efforts in obtaining a better wavefunction to describe a

given system, in DFT one is only interested in the one-electron density ρ given by

$$\rho(\vec{r}) = N_e \int \psi^* \psi \, \mathrm{d}\vec{r_2} \, \mathrm{d}\vec{r_3} \ldots \mathrm{d}\vec{r_N} \tag{2.62}$$

where N_e is the number of electrons. The electron density can be understood as the probability of finding any electron of the N_e electrons present in the system at a given position of space. Given the fact that ρ is a probability density, it is a non-negative function in the whole domain $(-\infty,\infty)$. The following properties of the electron density are highlighted:

1. $\lim_{r\to\infty} \rho = 0$, meaning that it is integrable.
2. $\int \rho(\vec{r_1}) \, \mathrm{d}\vec{r_1} = N_e$
3. The electron density has maxima only at the positions of the nuclei.

The origins of this method can be traced back to the Thomas-Fermi model from 1927 [38], where the energy of a fictitious system, the uniform electron gas was given in terms of solely the electron density

$$E_{TF}[\rho(\vec{r})] = \frac{3}{10}(3\pi^2)^{\frac{2}{3}} \int \rho^{\frac{5}{3}}(\vec{r}) \, \mathrm{d}\vec{r} - Z \int \frac{\rho}{r} \, \mathrm{d}\vec{r} + \frac{1}{2} \iint \frac{\rho(\vec{r_1})\rho(\vec{\rho_2})}{r_{12}} \, \mathrm{d}\vec{r_1} \, \mathrm{d}\vec{r_2} \tag{2.63}$$

where we distinguish the kinetic, nucleus-electron and electron-electron interaction energies respectively. The nucleus-electron interaction is system-dependent and is usually referred to as external potential V_{ext}. The kinetic and electron-electron functional forms are common to all systems. The electron-electron interaction can be separated in a classical contribution $J[\rho]$ and a non-classical part $E_{XC}[\rho]$ known as the exchange-correlation potential which takes into account the antisymmetry principle, self-interaction error and correlation effects, which as the kinetic energy functional is not known. The energy functional could then be written as

$$E[\rho] = T[\rho] + V_{ext}[\rho] + J[\rho] + E_{XC}[\rho] \tag{2.64}$$

The real advent of DFT as is known today came with Hohenberg-Kohn theorems stated in 1964, according to which [39]:

1. The external potential is a unique functional of $\rho(\vec{r})$; and since the external potential V_{ext} fixes $\hat{\mathcal{H}}$, the ground state energy of a many-particle system is a functional of the density.

2. The second Hohenberg-Kohn theorem states that the true density of the system delivers the lowest ground state energy, i.e., the search of the actual density of the system is a variational problem.

The previous theorems only ensure the existence of a unique ground state density which gives the lowest energy. However, they provide no recipe of how to construct the energy functional. This was solved with the appearance of the Kohn-Sham scheme [40], which considered a non-interacting fictitious system with the same density as the real one. It is therefore described by a Slater determinant and a set of orbitals, called the Kohn-Sham orbitals. The energy functional is then expressed in terms of the KS orbitals

$$E[\rho] = \frac{1}{2}\sum_{i}^{N_e} \langle \varphi_i | \nabla^2 | \varphi_i \rangle + \frac{1}{2}\sum_{i}^{N} {}_e \sum_{j}^{N_e} \iint |\varphi_i(\vec{r_1})|^2 \frac{1}{r_{12}} \left|\varphi_j(\vec{r_2})\right|^2 \mathrm{d}\vec{r_1}\, \mathrm{d}\vec{r_2} \tag{2.65}$$

$$+ E_{XC}[\rho] + \sum_{i}^{N_e}\sum_{A}^{N_n} \int \frac{Z_A}{r_{1A}} |\varphi_i(\vec{r_1})|^2 \, \mathrm{d}\vec{r_1} \tag{2.66}$$

The only unknown term from the previous equation is the $E_{XC}[\rho]$ functional. It includes exchange-correlation effects as well as the kinetic energy not included in the first term, which corresponds to a non-interacting system.

The problem is then reduced to finding the best KS orbitals φ_i that minimize the energy subject to the constraint $\langle \varphi_i | \varphi_j \rangle = \delta_{ij}$, analogously to the HF case. One arrives then to the one electron equations

$$\left(-\frac{1}{2}\nabla^2 + \left[\int \frac{\rho(\vec{r_2})}{r_{12}} \mathrm{d}\vec{r_2} + V_{\mathrm{XC}}(\vec{r_1}) - \sum_{A}^{N_n} \frac{Z_A}{r_{1A}} \right] \right) \varphi_i \tag{2.67}$$

$$\left(-\frac{1}{2} + V_{eff}(\vec{r_1}) \right) \varphi_i = \epsilon_i \varphi_i \tag{2.68}$$

which, when solved, yield the KS orbitals that minimize the energy, from which the electron density can be calculated in the same way as HF

$$\rho(\vec{r}) = \sum_{i}^{N_e}\sum_{j}^{N_e} \varphi_i^*(\vec{r})\varphi_i(\vec{r}) \tag{2.69}$$

It should be highlighted that the Kohn-Sham approximation is essentially exact. The approximation comes from the form chosen for the exchange-correlation

potential. Over the years many exchange-correlation functionals have been developed, but none of them is universal. One has to choose "wisely" the exchange-correlation functional to use depending on the system of interest.

The main advantage of DFT over classical wavefunction methods comes from using the electron density, since it is an object of just 3 space variables, while the wavefunction depends on 3N. The fact of dealing with an object of much lower dimensionality than the wavefunction has enabled the theoretical study of larger systems, not just molecules of a few atoms, but solids, nanostructures, proteins...

Chapter 3

Light-Matter Interaction. Photoionization methods

3.1 Gauge invariance. Photoionization cross sections

The interaction of a molecule with an electromagnetic field can be described rigorously by quantum electrodynamics, which treats the molecule or atom as well as the photons quantum mechanically. Nevertheless, it is common to use a semi-classical approach in which the molecule is described by quantum mechanics and interacts with a classical electromagnetic field, that does not consider photons as particles. This is the case for the methods we are employing in this work.

In this semi-classical approach the interaction energy $V(t)$ between a given system and electromagnetic radiation can be written in terms of position —length gauge— or momentum —velocity gauge—.

$$V(t) = \vec{r}\vec{E}(t) \quad \text{length gauge} \tag{3.1}$$

$$V(t) = \frac{1}{c}\vec{p}\vec{A}(t) \quad \text{velocity gauge} \tag{3.2}$$

where $\vec{E}(t)$ is the electric field and $\vec{A}(t)$ is the vector potential given by

$$\vec{E}(t) = \frac{\partial}{\partial t}\vec{A}(t) \tag{3.3}$$

The dipole coupling between initial Ψ_a and final Ψ_b states, which is related to the probability of transition, also depends on the gauge used.

$$M^L_{ab} = N_e \langle \Psi_a | \vec{\epsilon} r | \Psi_b \rangle \quad \text{length gauge} \tag{3.4}$$

$$M^V_{ab} = N_e \langle \Psi_a | \vec{\epsilon} \nabla | \Psi_b \rangle \quad \text{velocity gauge} \tag{3.5}$$

From the dipole couplings we can define a magnitude called single photoionization cross section, which denotes the probability a given photoionization event has to occur. At first order perturbation theory the cross section can be related related with the dipole transition as

$$\sigma_{ab}^{L} = 4\pi^2\alpha(E_b - E_a)\left|M_{ab}^{L}\right|^2 \quad \text{length gauge} \tag{3.6}$$

$$\sigma_{ab}^{V} = \frac{4\pi^2\alpha}{E_b - E_a}\left|M_{ab}^{V}\right|^2 \quad \text{velocity gauge} \tag{3.7}$$

α is the hyperfine structure factor ($\approx 1/137$) au and M_{ab} the dipole coupling, in its length and velocity form respectively. The result obtained should not depend on how we define the interaction with the electromagnetic field, be it in terms of momentum or position. This is generally known as gauge invariance, and it has been used to check the convergence of the XCHEM calculation.

3.2 Scattering states

Photoionization consists of the ejection of an electron from a molecule. The ejected electron behaves as a particle under the influence of a potential, the one created by the ion core. Therefore, photoionization is equivalent to the scattering of a particle. To model this system we make use of the radial TISE equation for one electron with solution $R_{nl}(r)$

$$\left[-\frac{1}{2r}\frac{\mathrm{d}^2}{\mathrm{d}r^2}r + \frac{l(l+1)}{2r^2} + V(r)\right] R_{nl}(r) = E_{nl}R_{nl}(r) \tag{3.8}$$

By focusing on the continuum spectrum of $\hat{\mathcal{H}}$ and considering $\kappa^2 = 2E$, $u_{\kappa l} = rR_{\kappa l}$ we cast Equation 3.8 into Equation 3.9

$$\left[\frac{\mathrm{d}^2}{\mathrm{d}r^2} + \kappa^2 - \frac{l(l+1)}{r^2} - U(r)\right] u_{\kappa l}(r) = 0 \tag{3.9}$$

If we consider the case $U(r) = 0$ for a sufficiently large r, we obtain the equation for a free particle

$$\left[\frac{\mathrm{d}^2}{\mathrm{d}r^2} + \kappa^2 - \frac{l(l+1)}{r^2}\right] u_{\kappa l}^{free}(r) = 0 \tag{3.10}$$

The solution to the free particle equation is expressed in terms of spherical Bessel functions j_l and n_l

$$u_{\kappa l} = A r j_l(\kappa r) + B r n_l(\kappa r) \tag{3.11}$$

where rj_l and rn_l are known as regular F_l and irregular G_l solutions. Spherical bessel functions are defined via

$$j_l(r) = (-1)^l \left(\frac{1}{r}\frac{\mathrm{d}}{\mathrm{d}r}\right)^l \frac{\sin(r)}{r} \tag{3.12}$$

$$n_l(r) = -(-1)^l \left(\frac{1}{r}\frac{\mathrm{d}}{\mathrm{d}r}\right)^l \frac{\cos(r)}{r} \tag{3.13}$$

The regular and irregular functions behave asymptotically when $r \to \infty$ as

$$F_l \to \sin\left(kr - \frac{l\pi}{2}\right) \tag{3.14}$$

$$G_l \to \cos\left(kr - \frac{l\pi}{2}\right) \tag{3.15}$$

n_l shows a divergence at $r = 0$ for all l, thence $B = 0$ in u_{kl}^{free}.

If we now consider a potential $U(r)$ up to a distance R_u, we need both j_l and n_l to obtain $u_{\kappa l}(r)|_{r>R_U}$ with the correct boundary conditions. In this case, at long distances we would obtain

$$u_{\kappa l}(r)|_{r>R_U} = A \sin\left(\kappa r - \frac{l\pi}{2}\right) + B \cos\left(\kappa r - \frac{l\pi}{2}\right) \tag{3.16}$$

$$= \sqrt{A^2 + B^2} \sin\left(\kappa r - \frac{l\pi}{2} + \delta_l\right) \tag{3.17}$$

We can see that in the presence of a potential, the scattered particle behaves at long distances exactly as a free particle except for the presence of a phase shift δ_l given by

$$\delta_l = \tan^{-1}(A/B) \tag{3.18}$$

The solution to a scattering problem can the be viewed as a superposition of free particles solutions, taking into account its corresponding phase shift.

Finally, we are considering the case the potential follows a coulomb law, i.e. $U(r) = \frac{1}{r}$. The solutions are called coulomb wavefunctions and are defined in terms of the hypergeometric functions. The regular and irregular solutions F_l

and G_l have the following asymptotic behavior

$$F_l(\kappa r, \eta) = \sin\left(\kappa r - \frac{\pi l}{2} + \sigma_l - \eta \log(2\kappa r)\right) \tag{3.19}$$

$$G_l(\kappa r, \eta) = \cos\left(\kappa r - \frac{\pi l}{2} + \sigma_l - \eta \log(2\kappa r)\right) \tag{3.20}$$

where σ_l is the coulomb phase shift. Coulomb wavefunctions play an important role in photoionization, since at long distances one can consider that the electron feels the ion as a coulomb potential.

3.2.1 B-splines basis

B-spline functions were introduced in the 40s by Schoenberg [41] and have been extensively used mainly in mathematical numerical analysis, and even in computer graphics. From the 90s they have entered in the atomic and molecular physics field thanks to their outstanding properties. They form an essentially complete basis set with a relatively low number of basis functions and negligible linear dependencies [42].

B-splines are piecewise polynomial functions that are defined in an interval $[a, b]$ by:

1. An order $k \in \mathbb{N}$.

2. A non-decreasing knot vector t that divides the interval $[a, b]$ in l subintervals by $l + 1$ knots. It is allowed to have knots with a multiplicity higher than 1, used to reduce continuity. Knot vectors are normally built up with a maximum k multiplicity at the endpoints and simple uniform knots in the interior leading to $t = (t_1, \ldots, t_1, t_2, t_3 \ldots, t_{l+1}, \ldots, t_{l+1})$. This knot vector is the one we will be considering. It contains a set of $l + k - 1$ B-splines and allows to set boundary conditions at the endpoints with the first B_1 and last B_n B-splines.

They are generated recursively by the De Boor algorithm [43]

$$B_i^k(r) = \frac{x - t_i}{t_{i+k-1} - t_i} B_i^{k-1}(r) + \frac{t_{i+k} - x}{t_{i+k} - t_{i+1}} B_{i+1}^{k-1}(r) \tag{3.21}$$

$$B_i^1(r) = \begin{cases} 1 & t_i \leq x \leq t_{i+1} \\ 0 & \text{otherwise} \end{cases} \tag{3.22}$$

where we can notice that a single B-spline is defined by $k+1$ knots (k subintervals) and

$$B_i(r) > 0 \quad \text{iff} \quad r \in]t_i, t_{i+k}[\tag{3.23}$$

$$B_i(r) = 0 \quad \text{iff} \quad r \notin [t_i, t_{i+k}] \tag{3.24}$$

Consequently, there are k non-zero B-splines in a given subinterval $[t_i, t_{i+k}]$ and the product of two B-splines follows

$$B_i^k \cdot B_j^k = 0 \quad \text{for} \quad |i-j| \geq k \tag{3.25}$$

yielding banded matrix representations with a $k-1$ bandwidth.

As it has already shown, continuum electrons have an asymptotic oscillatory nature, meaning that scattering functions are not square-integrable and do not belong to the $\mathcal{L}^2$ space. Given the fact that B-splines are defined in a finite box, they are square-integrable and allow for the normalizability of the wavefunction. They must be able to reproduce the oscillatory behavior of the electron and must match the boundary conditions at the end of the box.

3.3 Static-Exchange DFT

Decleva and collaborators [18, 19] developed a method that enables the calculation of dipole couplings between electronic states under the DFT formalism. This method has proved to provide precise photoionization cross sections for small and medium sized molecules within the fixed nuclei approximation

The method begins with a calculation of the ground state by using the ADF package [44] with the LB94 exchange-correlation functional [45]. This functional is designed to have the correct Coulomb-like asymptotic behavior. From this calculation we obtain the KS-orbitals for the ground state from which we obtain cationic one-hole states by removing one single electron and promoting it to a continuum orbital yielding N-electron wavefunction of the form

$$\psi^N(r) = \mathcal{A}\psi^{N_e-1}(r_1, r_2, \ldots r_{N-1})\varphi(r_N) \tag{3.26}$$

STO basis used in bound state electronic calculations provide a reasonable fast convergence and accuracy, but they are unsuited for the continuum. Therefore, the method uses a multicenter expansion of B-splines and spherical harmonics

in which to expand the electronic wavefunction. There are B-spline centers at each atomic position and also at the the center of mass of the molecule. The Hamiltonian of the system is constructed in this basis, and its diagonalization yields bound states, when their energy is lower than the ionization threshold, and discretized continuum states otherwise. Nevertheless, the obtained scattering states do not satisfy the correct boundary conditions. The actual scattering states are obtained by using the Galerkin approach, that allows to obtain them at the chosen energies.

3.4 XCHEM Methodology

3.4.1 GABS Basis

Traditional Quantum Chemistry Packages are based on Gaussian functions and they are not appropriate for describing continuum electrons. On the contrary, B-splines have been successfully used to describe the electronic continuum. That is why XCHEM has combined the best of two world in a hybrid approach by using Gaussian and B-spline functions in a unique basis called GABS. The GABS basis was introduced by Marante [13] and it was used to represent bound and continuum states of hydrogen, obtaining essentially exact results. It consists of a set of gaussian functions —monocentric gaussians (MC)— centered at the center of mass of the molecule with the form

$$G^{\alpha}_{klm}(r,\theta,\phi) = \sqrt{\frac{1}{2}}\left(\frac{\pi}{\alpha}\right)^{1/4}\sqrt{\frac{(4k+2l+1)!!}{(4\alpha)^{2k+l+1}}}r^{2k+l}e^{-\alpha r^2}Y_{lm}(\theta,\phi) \tag{3.27}$$

l is the angular momentum and k is included to provide a greater radial flexibility. The α exponents for each orbital angular momentum come from a geometric progression [46]

$$\alpha_n = \alpha\beta^{n-1} \tag{3.28}$$

The B-splines are constructed to begin at a certain radius R_0 that guarantees overlap with monocentric gaussians but no overlap with the polycentric basis coming from a quantum chemistry calculation.

In Figure 3.1 we show a representation of the GABS basis. The black dots at the center represent the polycentric gaussian basis (PC). On top of it we see the MC basis that extends effectively until a certain distance, represented by the blue area. Finally, we have the B-spline basis represented by the purple area and which

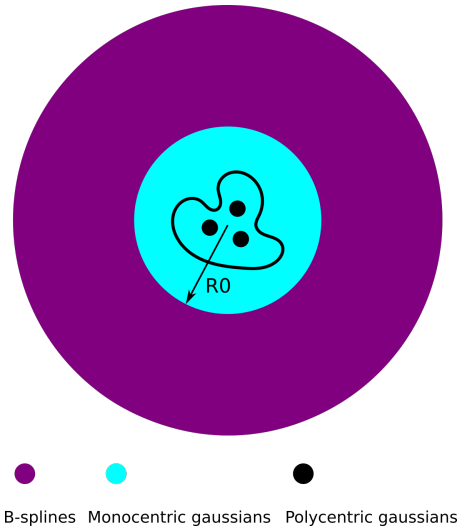

FIGURE 3.1: Scheme of the GABS basis. Adapted from [47].

starts at R_0 and extends to the end of the box. As it can be seen from the figure, B-splines do not overlap with the polycentric gassians and one does not have to bother with those kind of integrals. The connection between B-splines and MC is what permits the electron from the neutral molecule to go into the continuum, leaving the molecule ionized.

3.4.2 Augmentations

Firstly, the parent ions electronic states are obtained from a state-averaged CASSCF calculation. This ensures that they all have the same molecular orbitals, so that Slater-Condon rules Equation 2.15 and Equation 2.16 can be applied. The virtual orbitals are removed and substituted by the GABS basis. The virtual orbitals are very diffuse and can overlap with the B-splines, what is not allowed by the XCHEM model.

The wavefunction is then described in a Close Coupling expansion:

$$|\psi_E\rangle = \sum_i c_i^E |\psi_i\rangle + \sum_\alpha \sum_j c_{\alpha j}^E a_j^\dagger |\Phi_\alpha\rangle \tag{3.29}$$

where ψ_i represents the N_e electron wavefunctions that belongs to the neutral manifold, whereas the second part describes all possible augmentations of the different parent ions α in the orbital j. This augmentation is done in different orbital sets:

1. Augmentation in the remaining polycentric orbitals.

2. Augmentation in the monocentric orbitals.

3. Augmentation in the B-splines

The possibilities 1 and 2 imply only the use of Gaussian functions and they integrals between them are calculated using a modified version of the OpenMolcas package [11]. The last possibility is calculated by the XCHEM code considering that the overlap between B-splines and polycentric orbitals can be neglected. The augmentation on B-splines is done separating the radial and angular part, so that this part is defined by $|\Lambda_\alpha Y_{lm} R\rangle$, where Λ_α is the channel function associated with the parent ion Φ_α, the angular distribution of the B-spline is depicted by the spherical harmonics Y_{lm} and the radial part R is represented by B-splines.

Before finishing, a few comments on resonances and autoionizing states. The autoionizing states come from the augmentations, which yield N_e electron states in which the electron is far from the molecule and loosely bound. These autoionizing states are related to the parent ion from which they are built by augmentation of one electron. For each parent ion there is a set of bound states that converge to the parent ion energy, as shown in Figure 3.2. When this parent ions —channels— are coupled in a multi-channel calculation there is a possibility that ionization occurs by through the decay of an autoionizing state. The interference between this path and direct ionization gives rise to Fano resonance in the photoionization spectrum.

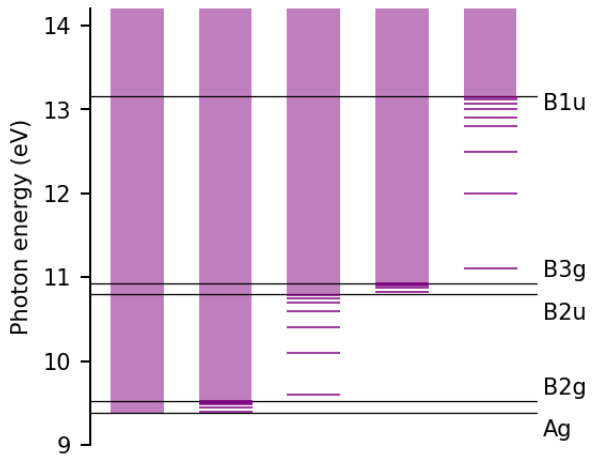

FIGURE 3.2: Schematic representation of the autoionizing states and continua of pyrazine. Ionization thresholds come from a CASSCF (9,8) calculation that will be addressed in chapter 4

The photoionization cross section in a shape resonance, i.e. when autoionizing states are not involved, follows a Lorentzian shape

$$\sigma(E) = \frac{\pi}{\kappa^2} \frac{\Gamma}{\frac{1}{4}\Gamma^2 + (E - E_R)^2} \tag{3.30}$$

where Γ is the width of the resonance and E_R its energy. This width is related to the lifetime by $\tau \propto \frac{1}{\Gamma}$. Therefore long lifetimes yield very narrow peaks in the photoionization spectrum. In case an autoionizing state is involved at this energy, the photoionization cross section changes to an asymmetric shape known as Fano profile [48].

Chapter 4

Results and Discussion

In this thesis we have used the XCHEM and DFT static-exchange methods, previously described, to obtain the ionization cross sections of the pyrazine molecule under the fixed nuclei approximation. This means that we are considering a unique geometry of pyrazine, that was obtained from a geometry optimization of the ground state at the MP2 level with a cc-PVTZ basis [49]. Nevertheless, one must be cautious, given the fact that nuclei move for sufficiently long times. Ultimately, we can only expect to trust results that come from very short lifetimes.

The main objective consists of performing a multi-channel calculation with the XCHEM method for pyrazine and analyze the resonances that may appear. Furthermore, we will compare the results given by the well-established method based on DFT with the ones given by XCHEM. The DFT static-exchange method does not allow for close-coupling of ionization channels, while XCHEM does. Therefore, in order to have a better comparison the XCHEM method has been adapted to obtain a single channel result. A multichannel calculation has also been performed in order to show why XCHEM will play an important role in describing and understanding photoionization.

Firstly, we will address the electronic structure calculation along with the parent ions considered in this project, and subsequently we will focus on the photoionization cross section curves obtained by both methods.

4.1 Bound electronic states

Prior to obtaining scattering states and cross sections, one must obtain the bound states for the neutral system as well as the cation. In the case of XCHEM this bound states are obtained from CASSCF, while in DFT static exchange come from a DFT calculation. We have considered the ground state of neutral and 5 electronic states of the cation.

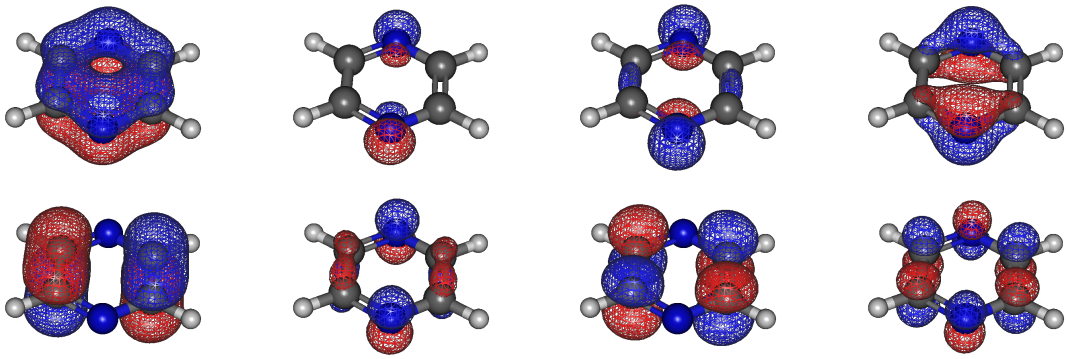

FIGURE 4.1: Molecular orbitals of pyrazine from a CASSCF (9,8) state-averaged calculation. First row: $6a_g$, $5b_{2u}$, $1b_{1u}$, $1b_{3g}$. Second row: $1b_{2g}$, $2b_{1u}$, $1a_u$, $2b_{3g}$.

4.1.1 Multireference methods

Regarding electronic structure, XCHEM permits a far more accurate description of bound states, since it uses CASSCF for this purpose. This means that bound states are described by several determinants, as many as the user desires, the only limitation being computer time availability; in contrast to DFT where bound states are described from a single Slater determinant.

The orbitals were calculated by averaging the wavefunction of the cation states, i.e. a SA5-CASSCF calculation and the neutral was obtained within these orbitals. In this project we have used two different active spaces: (9,5) and (9,8). The eight orbitals are represented in Figure 4.1, and as it can be seen they correspond to π, n and π^* orbitals. In fact, the active space (9,8) is fairly small but contains the necessary to describe the cationic states. From [50] one can see that the main cationic states of pyrazine are associated to ejecting electrons from π and n orbitals. Since pyrazine belongs to the D_{2h} symmetry group, the parent ions considered for this project are A_g, B_{2g}, B_{2u}, B_{3g} and B_{1u}.

The (9,5) active space does not contain the last three orbitals in Table 4.1, it just contemplates the occupied ones. This means that electronic states are built up with a single determinant. The purpose of using this active space is to mirror as much as possible the static-exchange method, and examine the effect of increasing the configuration space in the photoionization cross sections.

In Table 4.1 the results for the multiconfigurational calculations are shown. The MRCI was done on top of the (9,8) calculation. There is a clear decrease in the energy of all the considered states, however, the ionization thresholds for (9,8) are not that far from the MRCI, meaning that it is a valid active space. In the case of (9,5) we see that there are some big differences.

CASSCF (9,8)			all π, n, π^* orbitals		
Molecule	State	E_{MRCI} (au)	ΔE_{MRCI} (eV)	E (au)	ΔE (eV)
Pyrazine	^1A_g	-263.6462	0.000	-262.8226	0.000
[Pyrazine]$^+$	^2A_g	-263.2926	9.618	-262.5109	8.478
	$^2B_{2g}$	-263.2816	9.917	-262.5056	8.622
	$^2B_{2u}$	-263.2374	11.119	-262.4587	9.898
	$^2B_{3g}$	-263.2275	11.389	-262.4544	10.015
	$^2B_{1u}$	-263.1457	13.614	-262.3722	12.251
CASSCF (9,5)			only π, n orbitals		
Molecule	State		E (au)	ΔE (eV)	
Pyrazine	^1A_g		-262.7356	0.000	
[Pyrazine]$^+$	^2A_g		-262.3868	10.080	
	$^2B_{2g}$		-262.4245	9.055	
	$^2B_{2u}$		-262.3093	12.188	
	$^2B_{3g}$		-262.3658	10.652	
	$^2B_{1u}$		-262.2220	14.563	

TABLE 4.1: Energy results from the (9,8) and (9,5) CASSCF calculations and comparison with MRCI results

4.1.2 DFT

As opposed to the previous case, here we use the KS-orbtials from a ground state DFT calculation for neutral pyrazine. The ionic states are obtained by removing electrons from KS-orbitals, thus generating holes. In light of having a paired system, the one-electron holes yield cationic states of the same symmetry as the orbital where the hole was generated. We have only considered cationic states that mirror the states from the previous section. States with the same A_g, B_{2g}, B_{2u}, B_{3g} and B_{1u} symmetry and higher in energy, when several available for a given symmetry where selected.

In Figure 4.2 we show the cationic states energy relative to the ground state for the different methods employed. Considering MRCI as as the best option, we can observe that (9,8) yields a result qualitatively identical, maintaining the relative order of the cationic states. In the other methods, this is not the case, and we discern that the energy order changes for (9,5) and DFT.

In the MRCI calculation we have used neutral pyrazine orbitals, in other words, it is the best ground state that can be obtained; while for the (9,8) and (9,5) calculations we have used the ground state obtained by using the parent ions state-averaged orbitals. Still, for the computation of photoionization cross sections,

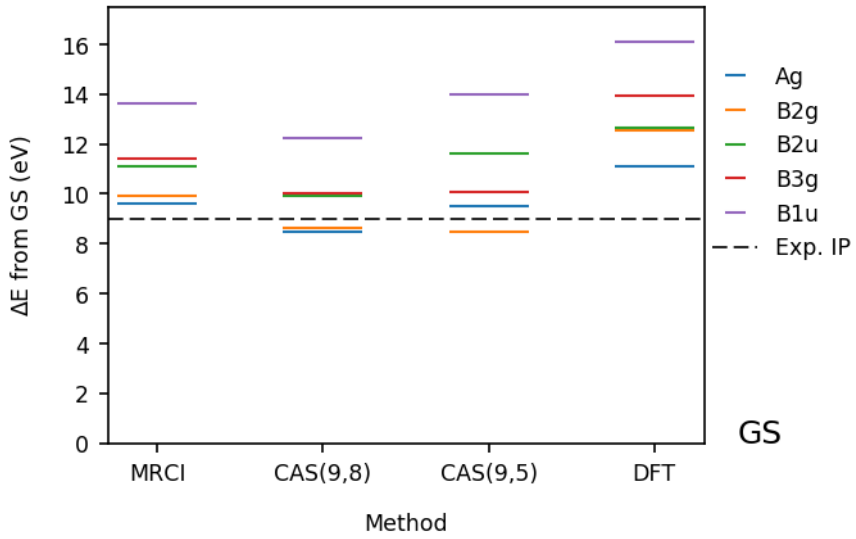

FIGURE 4.2: Cationic pyrazine states ralative to the ground state for different methods. Experimental ionization potential extracted from [51]

this is not the ground state used. As it has been described in chapter 3, we use a ground state that comes from augmenting the parent ions using the GABS basis. Thus, we obtain a better ground state, clearly with a lower energy. This results in a displacement to higher energies of the (9,8) and (9,5) cationic states relative to the GS. (9,8) first ionization threshold is already quite close to the experimental ionization potential; then if we take into account that there will be a slight increase in all the ionization thresholds thanks to a better description of the neutral ground state we could almost exactly reproduce the IP.

We can notice that for all methods except for (9,5) the ground state is of Ag symmetry. Therefore, (9,5) performs worse than DFT, as it could be foreseen, since DFT it not just a single determinant thanks to the inclusion of electron correlation through the exchange-correlation functional LB94.

4.2 Close Coupling scheme

In order to calculate photoionization cross sections one needs to calculate the dipole couplings between the ground state and the continuum states.

$$\langle \psi_{GS} | \vec{\epsilon} \hat{r} | \psi_E \rangle \tag{4.1}$$

TABLE 4.2: Close Coupling scheme. Symmetry of ejected electron and allowed l and m values for each parent ion and polarization direction.

Parent Ions		A_g	B_{2u}	B_{1u}	B_{2g}	B_{3g}
X	e^-	B_{3u}	B_{1g}	B_{2g}	B_{1u}	A_u
	l	1, 3, 5...	2, 4, 6...	2, 4, 6...	1, 3, 5, 7...	3, 5, 7...
	m	1, 3, 5...	-2, -4, -6...	1, 3, 5...	0, 2, 4...	-2, -4, -6...
Y	e^-	B_{2u}	A_g	B_{3g}	A_u	B_{1u}
	l	1, 3, 5...	0, 2, 4, 6...	2, 4, 6...	3, 5, 7...	1, 3, 5...
	m	-1, -3, -5...	0, 2, 4, 6...	-1, -3, -5...	-2, -4, -6...	0, 2, 4...
Z	e^-	B_{1u}	B_{3g}	A_g	B_{3u}	B_{2u}
	l	1, 3, 5...	2, 4, 6...	0, 2, 4, 6...	1, 3, 5, 7...	1, 3, 5...
	m	0, 2, 4...	-1, -3, -5...	0, 2, 4, 6...	1, 3, 5...	-1, -3, -5...

where ψ_e is constructed following the formula of Equation 3.29. The chosen channels are described by a parent ion channel Λ_α and the angular momentum of the B-splines Y_{lm}. In order for this integral to be non-zero, it must belong to the totally symmetric irreducible representation, A_g. The molecule of pyrazine is D_{2h}, and therefore the x, y and z components of the polarization vector have B_{3u}, B_{2u} and B_{1u} respectively. Taking into account that neutral pyrazine is A_g and the parent ions have A_g, B_2g, B_2u, B_3g and B_1u symmetry, depending on the polarization vector the ejected electron must belong to a certain irreducible representation, that will determine the allowed l and m, and thus the spherical harmonics employed in the close coupling expansion. In Table 4.2 we have gathered the valid l and m quantum numbers for the ejected electron depending on the polarization vector and the channel function, i.e. the final molecular ionic state.

4.3 DFT static exchange

First of all, a calculation for a maximum angular momentum of 8 is shown in Figure 4.3. We have represented the total cross section along with the partial cross sections from angular momenta 1, 3, 5 and 7. It can be observed that the lowest angular momenta $l = 1$ and $l = 3$ have higher contributions to the total cross section at low energies. The partial cross section for $l = 5$ and $l = 7$ are zero for near zero photoelectron energies. When the energy increases we discern a decrease in the cross sections associated with $l = 1$ and $l = 3$ and an increase

in $l = 5$. In the case of $l = 7$, it does not have a significant contribution in the interval of energies considered.

A convergence test have been done using the DFT static-exchange formalism, in order to know the lowest angular momentum needed to obtain reliable results. In Figure 4.4 we observe that $L = 3$ is clearly not enough and thus yields a structureless curve. By increasing the angular momentum one notes first the appearance of a peak and second its displacement to lower energies.

4.4 XCHEM

Now we are going to present the results obtained by the XCHEM method, by considering single and multichannel calculations and with two different active spaces. In all cases a box from 7.0 to 200 au with 390 B-splines of order $k = 7$ has been used.

In Figure 4.5 we compare the XCHEM single channel with the DFT method. Although, obviously not exactly equal we can recognize that XCHEM with just $l = 6$ and the active space (9,5) tries to reproduce the result that is obtained from the converged DFT calculation for $L_{max} = 18$ in the x direction. In the case of (9,8) we observe a single peak and displaced to higher energies. The fact that DFT and (9,5) are kind of similar and (9,8), with a much better description of the electronic structure, so different implies that a multireference calculation is important to describe the ionization of pyrazine.

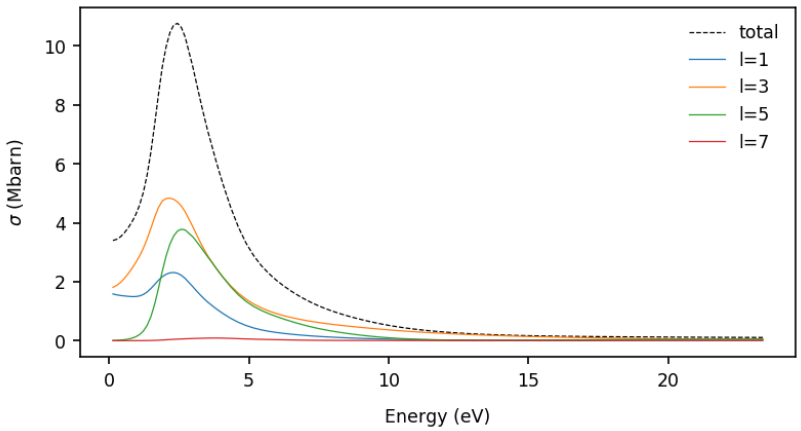

FIGURE 4.3: Partial cross sections for the transition ${}^1A_g \rightarrow {}^2A_g$ when $L_{max} = 8$.

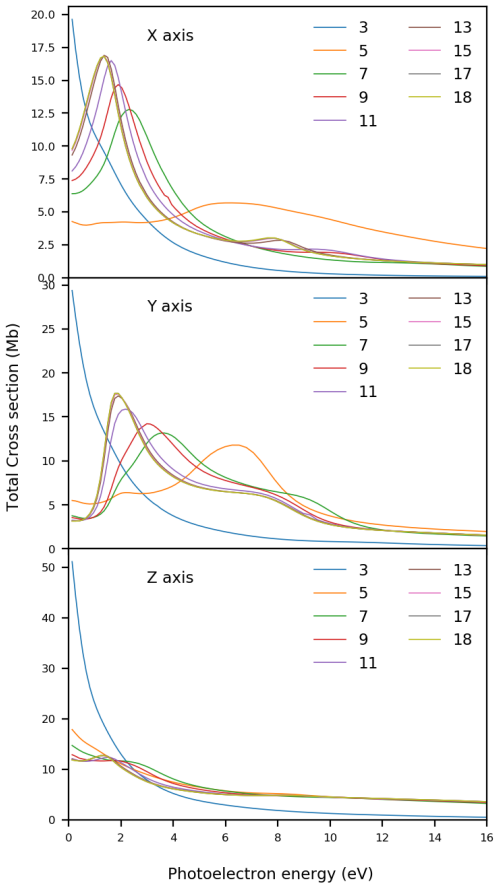

FIGURE 4.4: Total photoionization cross section for angular momentum 3–18.

For the y polarization we notice that both XCHEM calculations show a peak near 0.1 au. In the case of (9,8) we observe that there is some kind of structure above 0.2 au that is not observed in DFT and (9,5).

In the case of the z direction, DFT does not resemble at all the results obtained with both XCHEM calculations. In fact, the results obtained from (9,8) and (9,5) are quite similar, except for (9,8) displaying two small peaks.

In spite of not coinciding the scales, and in some cases obtaining different shapes this is quite an important result, since it means that in order to improve the XCHEM calculation and achieve convergence, there is no need to go to such large angular momentum values. Perhaps just including up to $L = 7$ or $L = 8$ is enough.

Finally, the results from a multichannel calculation in Figure 4.6 it can be observed there is a good agreement between the length and velocity gauges, meaning that the calculations have a certain degree of accuracy, although they could be

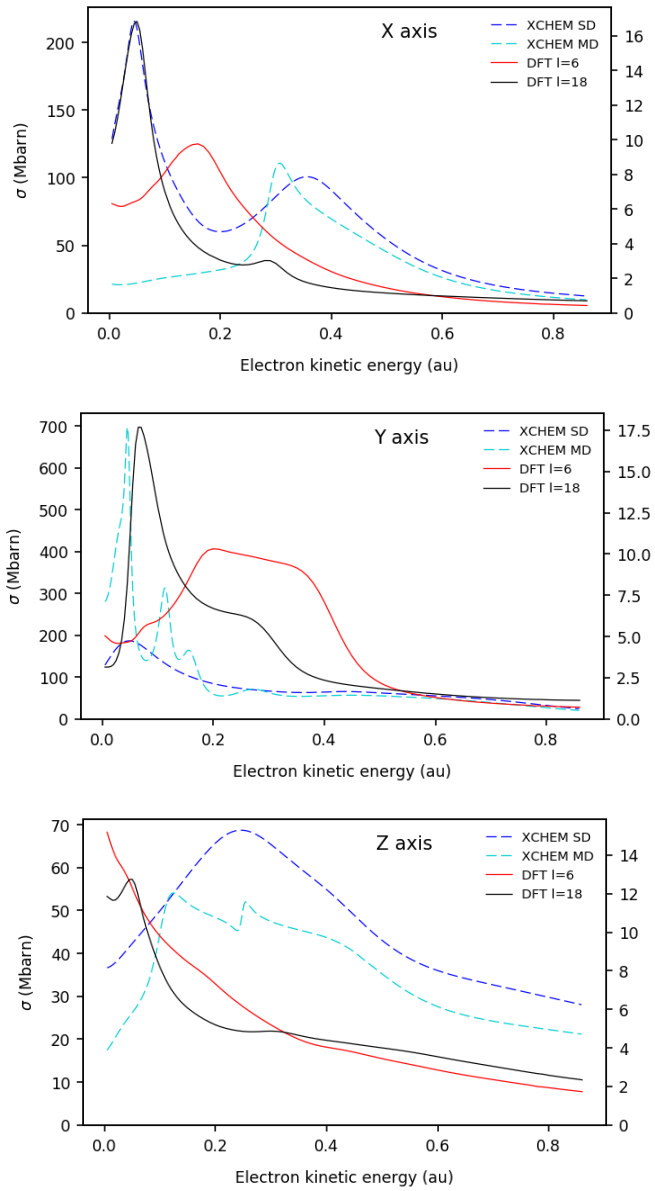

FIGURE 4.5: Comparison of XCHEM single channel calculations with active spaces (9,8) and (9,5) and $L = 6$ with DFT static-exchange $L = 6$ and $L = 18$.

improved. The outcome of this calculation is radically different from the ones obtained by considering only a single channel. We observe a series of peaks related to resonances that come from autoionizing states that decay to a given parent ion. These autoinizing states are present due to the fact that we are including a multichannel close coupling. Autoionizing states are a set quasi-bound states that converge to a given parent ion. In the XCHEM formalism they come from augmenting the parent ions. An excitation from the ground state to an autoionizing state associated to a given parent is followed by its decay to a parent ion of lower

energy. This is only possible to simulate by including several ionic channels in the Close Coupling expansion.

In Figure 4.6 we have summed the contributions to the total cross section per channel. This means that we observe to which parent ion the resonances are decaying. However, we cannot still know the origin of the resonance, i.e. the autoionizing state that eventually decays.

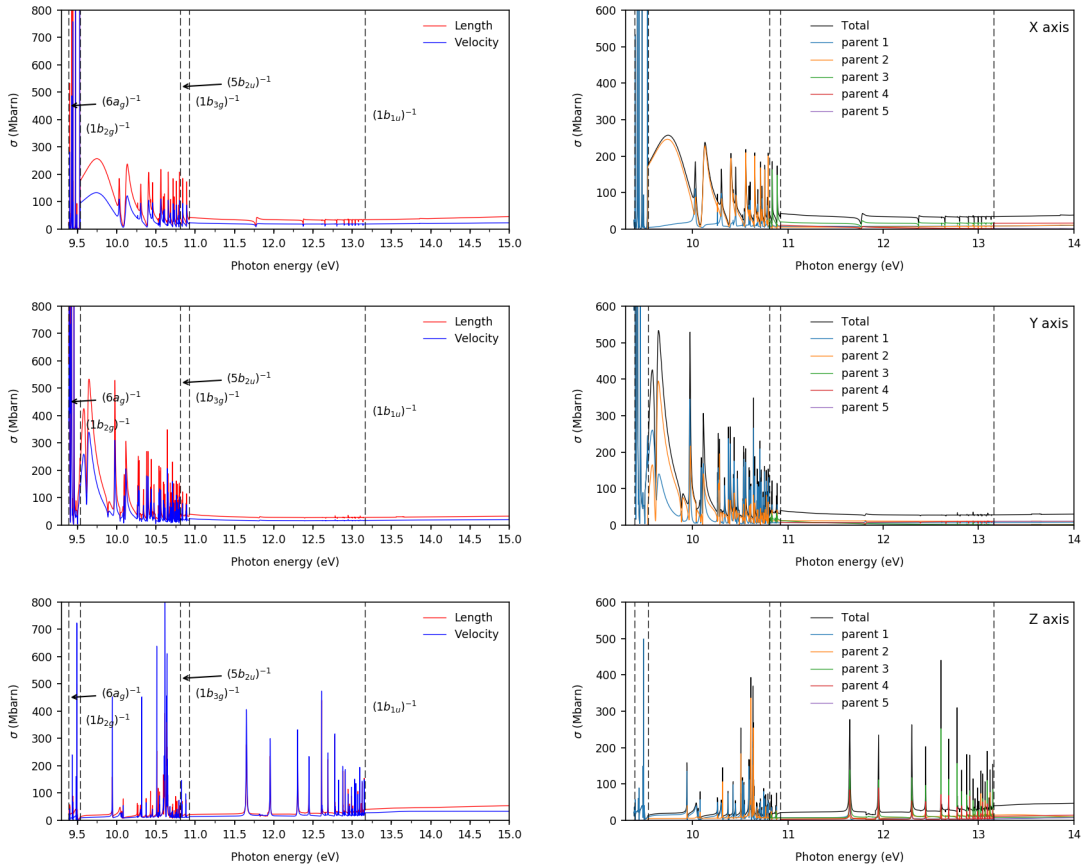

FIGURE 4.6: On the left: comparison of length and velocity gauges for a multideterminant and multichannel calculation. On the right: Channel contributions to the total photoionization cross sections. The dashed lines represent the ionization thresholds. Parent ions in energy order.

Below the second threshold there can only be decay to the lowest parent ion A_g, since it is the only open channel. Furthermore, for x and y polarizations we observe very thin peaks, meaning that they have long lifetimes and the fixed nuclei approximation is not holding. Between the second and third thresholds we observe wider peaks with contributions of both the first and second parent ions A_g and B_{2g}. The longer lifetimes of this resonances make them object of future study. In the case the z polarization, we have obtained a cleaner spectrum with

wider peaks and a noticeable decay to the third and fourth parent ions, in contrast with the other polarizations where decay occurs almost exclusively to parent ions A_g and B_{2g}. From the fourth to the fifth threshold we know that the resonances come from rydberg states associated to the fifth parent ion B_{1u}. Finally, there is no decay to the fifth parent ion since there are no autoionizing states above it.

Conclusions and Future prospects

In this work we have carried out a multi-channel calculation for the pyrazine molecule using a (9,8) active space. It has been shown a good agreement between the length and velocity gauges for this calculation and the channels that contribute to the total cross sections. As it has been stated, we cannot trust very narrow resonances, due to their long lifetimes. In the case of the x and y directions we intend to deepen in the resonances between the second and third thresholds that decay to the A_g and B_{2g} parent ions, but we still do not know where they come from. In the case of the z direction, we have observed wider and better defined resonances. The identification of resonances is now a development that we are introducing in the XCHEM code.

We have also calculated photoionization cross sections for the single-channel case with active spaces (9,8) and (9,5). The results obtained have been compared with the ones obtained from the static-exchange method. We have seen that the agreement is far from perfect, specially from the scale viewpoint. Nevertheless, we have observed that for $L = 6$, XCHEM already yields peaks near the positions given by SEA. This is an important result, meaning that XCHEM does not need to include so large angular momenta to achieve convergence.

Bibliography

[1] Ferenc Krausz and Misha Ivanov. "Attosecond physics". In: *Reviews of Modern Physics* 81.1 (2009), pp. 163–234. DOI: 10.1103/RevModPhys.81.163.

[2] Ahmed H. Zewail. "Femtochemistry: Recent progress in studies of dynamics and control of reactions and their transition states". In: *Journal of Physical Chemistry* 100.31 (1996), pp. 12701–12724. DOI: 10.1021/jp960658s.

[3] Ahmed H. Zewail. "Femtochemistry: Atomic-Scale Dynamics of the Chemical Bond†". In: (2000). DOI: 10.1021/JP001460H.

[4] P. B. Corkum. "Plasma perspective on strong field multiphoton ionization". In: *Physical Review Letters* 71.13 (1993), pp. 1994–1997. DOI: 10.1103/PhysRevLett.71.1994.

[5] Mauro Nisoli et al. "Attosecond Electron Dynamics in Molecules". In: *Chemical Reviews* 117.16 (2017), pp. 10760–10825. DOI: 10.1021/acs.chemrev.6b00453.

[6] D. Ayuso et al. "Dissociative and non-dissociative photoionization of molecular fluorine from inner and valence shells". In: *Journal of Electron Spectroscopy and Related Phenomena* 195 (2014), pp. 320–326. DOI: 10.1016/J.ELSPEC.2013.11.014.

[7] E. Kukk et al. "Effects of molecular potential and geometry on atomic core-level photoemission over an extended energy range: The case study of the CO molecule". In: *Physical Review A* 88.3 (2013), p. 033412. DOI: 10.1103/PhysRevA.88.033412.

[8] K Ueda et al. "Intramolecular photoelectron diffraction in the gas phase". In: *The Journal of Chemical Physics* 139.12 (2013), p. 124306. DOI: 10.1063/1.4820814.

[9] Philip G. Burke and Harry M. Schey. "Polarization and Correlation of Electron Spin in Low-Energy Elastic Electron-Hydrogen Collisions". In: *Physical Review* 126.1 (1962), pp. 163–168. DOI: 10.1103/PhysRev.126.163.

[10] Carlos Marante et al. “Photoionization using the xchem approach: Total and partial cross sections of Ne and resonance parameters above the 2 s 2 2 p 5 threshold”. In: *Physical Review A* 96.2 (2017), p. 022507. DOI: 10.1103/PhysRevA.96.022507.

[11] Francesco Aquilante et al. “Molcas 8: New capabilities for multiconfigurational quantum chemical calculations across the periodic table”. In: *Journal of Computational Chemistry* 37.5 (2016), pp. 506–541. DOI: 10.1002/jcc.24221.

[12] Hans-Joachim Werner et al. “Molpro: a general-purpose quantum chemistry program package”. In: *Wiley Interdisciplinary Reviews: Computational Molecular Science* 2.2 (2012), pp. 242–253. DOI: 10.1002/wcms.82.

[13] Carlos Marante, Luca Argenti, and Fernando Martín. “Hybrid Gaussian– B -spline basis for the electronic continuum: Photoionization of atomic hydrogen”. In: *Physical Review A* 90.1 (2014), p. 012506. DOI: 10.1103/PhysRevA.90.012506.

[14] Vinay Pramod Majety and Armin Scrinzi. “Dynamic Exchange in the Strong Field Ionization of Molecules”. In: *Physical Review Letters* 115.10 (2015), p. 103002. DOI: 10.1103/PhysRevLett.115.103002.

[15] Vinay Majety and Armin Scrinzi. “Photo-Ionization of Noble Gases: A Demonstration of Hybrid Coupled Channels Approach”. In: *Photonics* 2.4 (2015), pp. 93–103. DOI: 10.3390/photonics2010093.

[16] T. N. Rescigno et al. “Hybrid approach to molecular continuum processes combining Gaussian basis functions and the discrete variable representation”. In: *Physical Review A* 72.5 (2005), p. 052709. DOI: 10.1103/PhysRevA.72.052709.

[17] Thanh-Tung Nguyen-Dang et al. “Time-dependent quantum chemistry of laser driven many-electron molecules”. In: *Journal of Chemical Physics* 141.24 (2014), p. 244116. DOI: 10.1063/1.4904102.

[18] D Toffoli et al. “Convergence of the multicenter B-spline DFT approach for the continuum”. In: *Chemical Physics* 276.1 (2002), pp. 25–43. DOI: 10.1016/S0301-0104(01)00549-3.

[19] M. Venuti, M. Stener, and P. Decleva. “Valence photoionization of C6H6 by the B-spline one-centre expansion density functional method”. In: *Chemical Physics* 234.1-3 (1998), pp. 95–109. DOI: 10.1016/S0301-0104(98)00179-7.

[20] Albert Messiah. *Quantum Mechanics*. Dover Publications, 1980, p. 1136. ISBN: 0486409244.

[21] Christopher J. Cramer. *Essentials of computational chemistry : theories and models*. Wiley, 2004, p. 596. ISBN: 0470091827.

[22] Attila Szabo and Neil S. Ostlund. *Modern quantum chemistry : introduction to advanced electronic structure theory*. Dover Publications, 1996, p. 466. ISBN: 0486691861.

[23] C. C. J. Roothaan. "New Developments in Molecular Orbital Theory". In: *Reviews of Modern Physics* 23.2 (1951), pp. 69–89. DOI: 10.1103/RevModPhys.23.69.

[24] Trygve Helgaker, Poul Jørgensen, and Jeppe Olsen. *Molecular Electronic-Structure Theory*. Chichester, UK: John Wiley & Sons, Ltd, 2000. ISBN: 9781119019572. DOI: 10.1002/9781119019572.

[25] O Sinanoğlu. "MANY-ELECTRON THEORY OF ATOMS AND MOLECULES." In: *Proceedings of the National Academy of Sciences of the United States of America* 47.8 (1961), pp. 1217–26.

[26] R. K. Nesbet. "Electronic pair correlation in atoms and molecules". In: *International Journal of Quantum Chemistry* 5.S4 (2009), pp. 117–125. DOI: 10.1002/qua.560050710.

[27] J Cizek and J Paldus. "Coupled Cluster Approach". In: *Physica Scripta* 21.3-4 (1980), pp. 251–254. DOI: 10.1088/0031-8949/21/3-4/006.

[28] Isaiah Shavitt. "Graph theoretical concepts for the unitary group approach to the many???electron correlation problem". In: *International Journal of Quantum Chemistry* 12.11 S (1977), pp. 131–148. DOI: 10.1002/qua.560120819.

[29] Isaiah Shavitt. "Matrix element evaluation in the unitary group approach to the electron correlation problem". In: *International Journal of Quantum Chemistry Symposium* 12.S12 (1978), pp. 5–32. DOI: 10.1002/qua.560140803.

[30] K. Ruedenberg, L. M. Cheung, and S. T. Elbert. "MCSCF optimization through combined use of natural orbitals and the brillouin-levy-berthier theorem". In: *International Journal of Quantum Chemistry* 16.5 (1979), pp. 1069–1101. DOI: 10.1002/qua.560160511.

[31] Björn O. Roos. "The complete active space SCF method in a fock-matrix-based super-CI formulation". In: *International Journal of Quantum Chemistry* 18.14 S (1980), pp. 175–189. DOI: 10.1002/qua.560180822.

[32] Jeppe Olsen et al. “Determinant based configuration interaction algorithms for complete and restricted configuration interaction spaces”. In: *The Journal of Chemical Physics* 89.4 (1988), pp. 2185–2192. DOI: 10.1063/1.455063.

[33] Per Åke Malmqvist, Alistair Rendell, and Björn O. Roos. “The restricted active space self-consistent-field method, implemented with a split graph unitary group approach”. In: *Journal of Physical Chemistry* 94.14 (1990), pp. 5477–5482. DOI: 10.1021/j100377a011.

[34] Peter J. Knowles and Hans-Joachim Werner. “An efficient method for the evaluation of coupling coefficients in configuration interaction calculations”. In: *Chemical Physics Letters* 145.6 (1988), pp. 514–522. DOI: 10.1016/0009-2614(88)87412-8.

[35] Peter J. Knowles and Hans Joachim Werner. “Internally contracted multiconfiguration-reference configuration interaction calculations for excited states”. In: *Theoretica Chimica Acta* 84.1-2 (1992), pp. 95–103. DOI: 10.1007/BF01117405.

[36] Hans Joachim Werner and Peter J. Knowles. “An efficient internally contracted multiconfiguration-reference configuration interaction method”. In: *The Journal of Chemical Physics* 89.9 (1988), pp. 5803–5814. DOI: 10.1063/1.455556.

[37] Kerstin. Andersson et al. “Second-order perturbation theory with a CASSCF reference function”. In: *Journal of Physical Chemistry* 94.14 (1990), pp. 5483–5488. DOI: 10.1021/j100377a012.

[38] Wolfram Koch and Max C. Holthausen. *A Chemist's Guide to Density Functional Theory*. Weinheim, FRG: Wiley-VCH Verlag GmbH, 2001. ISBN: 3527303723. DOI: 10.1002/3527600043.

[39] P. Hohenberg and W. Kohn. “Inhomogeneous Electron Gas”. In: *Physical Review* 136.3B (1964), B864–B871. DOI: 10.1103/PhysRev.136.B864.

[40] W. Kohn and L. J. Sham. “Self-consistent equations including exchange and correlation effects”. In: *Physical Review* 140.4A (1965), A1133–A1138. DOI: 10.1103/PhysRev.140.A1133. arXiv: PhysRev.140.A1133 [10.1103].

[41] I. J. Schoenberg. “Contributions to the problem of approximation of equidistant data by analytic functions: Part B. On the problem of osculatory interpolation. A second class of analytic approximation formulae”. In: *Quarterly of Applied Mathematics* 4.1 (1946), pp. 112–141. DOI: 10.1090/qam/15914.

[42] H Bachau et al. “Applications of B -splines in atomic and molecular physics”. In: *Reports on Progress in Physics* 64.12 (2001), pp. 1815–1943. DOI: 10.1088/0034-4885/64/12/205.

[43] J. R. and Carl de Boor. “A Practical Guide to Splines.” In: *Mathematics of Computation* 34.149 (1980), p. 325. DOI: 10.2307/2006241. arXiv: 1501.02634.

[44] G. te Velde et al. “Chemistry with ADF”. In: *Journal of Computational Chemistry* 22.9 (2001), pp. 931–967. DOI: 10.1002/jcc.1056.

[45] R. van Leeuwen and E. J. Baerends. “Exchange-correlation potential with correct asymptotic behavior”. In: *Physical Review A* 49.4 (1994), pp. 2421–2431. DOI: 10.1103/PhysRevA.49.2421.

[46] A. Macías et al. “Simple discretization method for autoionization widths. III. Molecules”. In: *Physical Review A* 36.9 (1987), pp. 4203–4211. DOI: 10.1103/PhysRevA.36.4203.

[47] Carlos Marante et al. “Hybrid-Basis Close-Coupling Interface to Quantum Chemistry Packages for the Treatment of Ionization Problems”. In: *Journal of Chemical Theory and Computation* 13.2 (2017), pp. 499–514. DOI: 10.1021/acs.jctc.6b00907.

[48] U. Fano. “Effects of Configuration Interaction on Intensities and Phase Shifts”. In: *Phys. Rev.* 124 (6 1961), pp. 1866–1878. DOI: 10.1103/PhysRev.124.1866.

[49] Thom H. Dunning. “Gaussian Basis Functions for Use in Molecular Calculations. I. Contraction of (9s5p) Atomic Basis Sets for the First-Row Atoms”. In: *The Journal of Chemical Physics* 53.7 (1970), pp. 2823–2833. DOI: 10.1063/1.1674408.

[50] L. Åsbrink et al. “Rydberg series in small molecules: XVI. Photoelectron, uv, mass and electron impact spectra of pyrimidine”. In: *International Journal of Mass Spectrometry and Ion Physics* 8.3 (1972), pp. 215–227. DOI: 10.1016/0020-7381(72)80011-1.

[51] M. N. Piancastelli, P. R. Keller, and J. W. Taylor. “Angular distribution parameter as a function of photon energy for some mono- and diazabenzenes and its use for orbital assignment”. In: *Journal of the American Chemical Society* 105.13 (1983), pp. 4235–4239. DOI: 10.1021/ja00351a019.